TU Delft

Master Thesis

Stan Greveling - 4983920

Delft, February 11, 2022

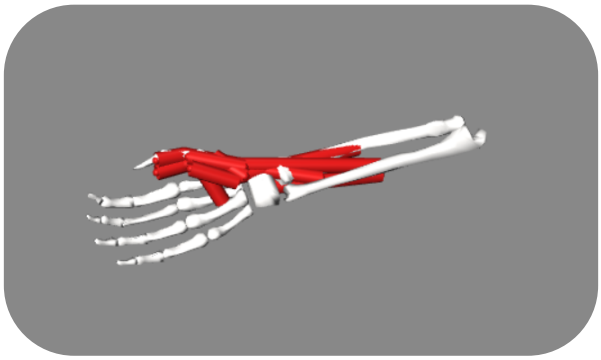

Comparing sEMG to estimated muscle force for the thumb muscles in the Delft Hand and Wrist model in OpenSim

Stan Greveling 4983920
Supervisors: Jinne E. Geelen and Winfred Mugge

***Abstract*—The Delft Hand and Wrist model is a recently created musculoskeletal model in the OpenSim environment. The current model lacks a validation of the thumb muscles. Therefore, the main goal of this work is to perform a quantitative trend validation by analyzing the correlation between experimentally measured muscle activity data and muscle forces estimated by the model from markerless motion capture data. The original model is reduced to a minimal model containing only the thumb muscles. A second model is created by changing optimal muscle fiber length, maximum isometric force and tendon slack length parameter values in the minimal model to values reported in literature to evaluate the effects of these adjustments on the estimated muscle force. An experiment is conducted in which participants are instructed to perform repetitive thumb motions while muscle activity and 2D kinematic data is captured. 3D kinematics are obtained through the machine learning toolboxes DeepLabCut and Anipose. Muscle forces are estimated through inverse dynamic static optimization in OpenSim. The results showed that the correlation between the estimated muscle forces and experimentally measured muscle activity data for both the minimal model and the adjusted model was very low to moderate, meaning both models yield unrealistic muscle force estimations. In contrast, the measured muscle activity and kinematic data show expected results thus are captured correctly, which is useful for reference in future work.**

There is room for improvement of the Delft Hand and Wrist model. Nevertheless, this work provides suggestions for the optimization of the current model and paves the way towards muscle force estimation and quantitative validation using experimentally measured muscle activity data for the Delft Hand and Wrist model in OpenSim.

***Index terms*—Inverse Dynamics, Muscle Force Estimation, Musculoskeletal Model, OpenSim, Static Optimization, Surface EMG, Thumb Kinematics, Thumb Muscles, Validation**

I. Introduction

The human hand contains 27 bones and over 30 muscles and is, due to its complexity, a popular research topic in biomechanics and robotics [1]. In particular, understanding human hand dynamics is required to develop and improve assistive devices, such as orthoses and exoskeletons [2]. These assistive devices help with the rehabilitation of hand impairments, for example after stroke [3], from which annually 15 million people suffer worldwide [4]. A better understanding of human hand dynamics is also desired for teaching purposes, e.g., surgeons in training or anatomy students, or for surgical planning, such as tendon transfers or joint replacements [5].

Performing experiments is one way to increase our knowledge regarding human hand functioning. However, understanding human hand functioning just by performing experiments is difficult because certain variables, such as generated muscle forces and muscle moment arms, are hard or impossible to measure directly during experiments without using invasive methods [6]. Muscle forces play a central role in coupling net joint moments to the underlying neurological control, while muscle moment arms affect the contribution of a muscle to the net joint moment [7]. This makes the muscle forces and muscle moment arms important variables for analyzing musculoskeletal behavior. An inverse dynamics approach combined with static optimization is frequently used to estimate muscle forces [8]. This approach uses measured kinematics and external forces to generate net joint moments [9]. In general, more muscles are crossing a joint than theoretically required to perform all possible movements of the joint. Static optimization is performed to solve this load sharing problem, i.e., the distribution of muscle force to muscles surrounding the joint according to the minimization of a predefined objective function in a way that joint equilibrium is satisfied [10].

The Delft Hand and Wrist model is a musculoskeletal model available in the OpenSim environment [11]. OpenSim is a computer simulation environment that allows for musculoskeletal modelling, inverse dynamic simulation of movement and static optimization [12]. The musculoskeletal model, retrieved from Mirakhorlo et al. (2018), is based on anatomical data of a single cadaver [13]. The resulting model contains a total of 43 muscles located in the hand, wrist and forearm and combined has 23 degrees of freedom at the joints. The muscles in the Delft Hand and Wrist model are Hill-type muscles based on the work of Thelen et al. (2003) [14]. The model was validated by comparing computed muscle moment arm values of the index finger to experimental values reported in literature, as well as comparing computed muscle forces during a pinch task to measured intraoperative reference forces. The validation method is valid but incomplete, because it only covers the index finger. The thumb differs from the other four fingers regarding bone composition, functional movements and orientation [15]. Therefore, the thumb should be validated separately.

Surface electromyography (sEMG) can be used for the validation of estimated muscle forces [16]. While qualitative comparison of measured muscle activity data to estimated muscle forces in terms of signal on- and offset exists [17], [18], only few studies focus on quantitative comparison described by a metric. In this work, an experiment is conducted in which captured motion data is used to estimate muscle forces using inverse-dynamics-based static optimization. The results are quantitatively validated by comparing the estimated muscle forces to simultaneously measured muscle activity.

The aim of this work is twofold. First; perform a quantitative

*Stan Greveling is with the Department of BioMechanical Engineering, Faculty of Mechanical, Maritime and Materials Engineering, Delft University of Technology, The Netherlands (email: stan.greveling@gmail.com)

validation of the thumb muscles using the Pearson correlation coefficient. Second; find out the effect of changing musculoskeletal parameters of the thumb muscles in the model to reference values reported in literature on the estimated muscle forces, hereby evaluating the sensitivity of the model. To achieve the goals of this work the following research questions have to be answered:
(1) Do the estimated muscle forces of the thumb in the Delft Hand and Wrist model obtained through inverse dynamic static optimization in OpenSim achieve a high correlation ($r \geq 0.6$) towards simultaneously measured muscle activity?
(2) How does changing the values for the maximum isometric force, tendon slack length and optimal muscle fiber length for the muscles in the Delft Hand and Wrist model to values reported in literature affect correlation between estimated muscle forces and the experimental muscle activity data?

The hypothesis is that a high correlation can be achieved for the current model, based on the findings in Mirakhorlo et al. (2018) [11]. Also, a higher correlation is expected when changing the maximum isometric force, tendon slack length and optimal muscle fiber length values to values reported in literature. Ultimately, the goal of this work is to provide a foundation for future work that aims to make the Delft Hand and Wrist model available online and open for access to use for academic purposes.

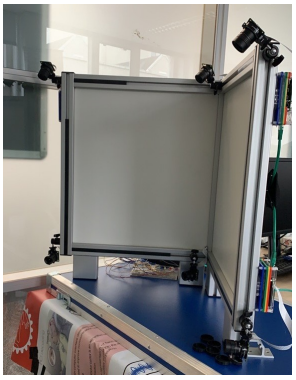

Fig. 1: The camera system (ML-MoCap).

Fig. 2: Complete experimental setup, including a participant.

II. Methods

Participants

A total of 18 participants participated in this experiment, of which seven are female and 11 male. Mean $\pm$ standard deviation of participant age is 28.1 ± 10.5 years. The participants that participated do not suffer from a recent hand injury that could affect their thumb motion. Two participants are left-handed, but the muscle activity and motion of the right arm was captured because the hand and wrist model in OpenSim is a model of the right arm. All participants signed Informed Consent forms prior to the experiments. The experiment is approved by the Human Research Ethics Committee of Delft University of Technology (approval number: 785).

Materials

A. Experimental setup

Thumb motion is recorded using a camera system that includes six cameras positioned in various angles, known as MarkerLess Motion Capture (ML-MoCap) [19], see Figure 1. Muscle activity is measured using the TMSi Porti7 system. Figure 2 shows the complete experimental setup including the electrodes of the TMSi Porti7 system attached to the arm of a participant.

B. Muscle activity

The TMSi Porti7 system uses wired micro-electrodes placed on the surface of the skin to measure muscle activity of the smaller muscles located in the hand and forearm. There is not enough space on the skin around the thumb to allow for bipolar sEMG electrode placement, so the muscle activity is measured unipolar. The potential difference between the micro-electrode and a ground electrode is recorded and provided to the amplifier. The ground electrode functions as the reference unit and is placed on the skin directly above the ulnar styloid because of the absence of muscle activity in this particular location. The sEMG electrodes are placed on the skin directly above the bellies of the eight muscles responsible for thumb movement. Table A1 in the Appendix displays these muscles and their characteristics. The muscle bellies are located through manual palpation according to the guidelines of the SENIAM project [20] and instruction videos by vhdissector [21]. The locations of the muscle bellies are marked and the skin is prepared for measurement by removing hair, cleaning the skin with alcohol and applying conductive gel before placing the electrodes. Figure 3 shows the electrodes attached on the participants arm. Once the electrodes are placed, a single maximum voluntary contraction (MVC) measurement is performed for normalization of the experimental data. The MVC measurement consists of performing maximal flexion, extension, abduction, and adduction of the thumb against manual resistance applied by the experimenter for three seconds. These movements together describe all possible movement directions of the thumb.

C. Kinematic data

Motion is captured using a frame rate of 30 Hz. The camera system sends a trigger signal to the TMSi system at the start of each trial to synchronize the muscle activity data and the kinematic data. The following thumb motions are recorded separately after the MVC measurement:

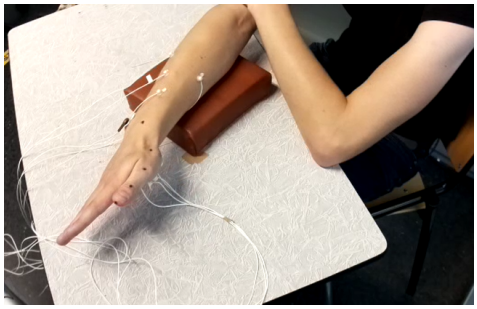

Fig. 3: The wired sEMG electrodes attached to the right arm of a participant. Black dots on the thumb indicate marker locations used for labeling in the DeepLabCut software.

- **Flexion/Extension (FE)**: The participant is requested to perform full flexion followed by full extension, for 10 repetitions.
- **Abduction/Adduction (AA)**: The participant is requested to perform full abduction followed by full adduction, for 10 repetitions.
- **IP Flexion/Extension (IP)**: The participant is requested to perform full flexion of the tip of the thumb followed by full extension of the tip of the thumb, for 10 repetitions.
- **Opposition (OPP)**: The participant is requested to perform opposition of the thumb without moving the other four fingers, for 10 repetitions.
- **Circular motion (Circle)**: The participant is requested to perform a circular motion of the thumb, for five clockwise rotations followed by five counter-clockwise rotations.

The participants are instructed to keep their right arm relaxed on the table while the back of their hand faces the cameras at all times. Figure 3 shows this neutral position recorded by camera 1. The neutral position is the starting position before each measurement.

D. Calibration

The camera system is calibrated by recording small movements of a ChArUco board with known marker sizes to achieve conversion from the kinematic data in Anipose from 2D to 3D. The ChArUco board is turned towards each camera and small rotational and translational movements are executed to ensure that the board is visible for all cameras. The cameras are calibrated in Anipose using a method called iterative bundle adjustment. The method minimizes the reprojection error, a metric that describes the resemblence of the 3D projections based on the 2D detections for each camera [22]. The maximum reprojection error among all calibration files used in this work is 0.52 pixels, which is below the threshold of 1 pixel as recommended in Karashchuk et al. (2021) [23].

Delft Hand and Wrist model

A. Minimal model

The original Delft Hand and Wrist model in OpenSim 4.1 is reduced to a minimal version containing only the muscles controlling the thumb. The reduction of muscles is done because the Static Optimization tool in OpenSim fails to find a feasible result when simulating the original model. Bringing the original model down to the most important components by selecting only the muscles that control the thumb and remove the two wrapping surfaces helps to understand and evaluate this issue. The two wrapping surfaces included in the original model that are removed were located at the first interphalangeal joint and first metacarpophalangeal joint. The muscle part that best suits the origin and insertion as represented in Table A1 is selected for the minimal model if multiple parts of this muscle existed in the original model. An exception is made for the Adductor Pollicis muscle, for which two parts are selected because of the muscle's two heads (one part for the transverse head and the other for the oblique head). Figure 4 shows the remaining muscles in the minimal Delft Hand and Wrist model.

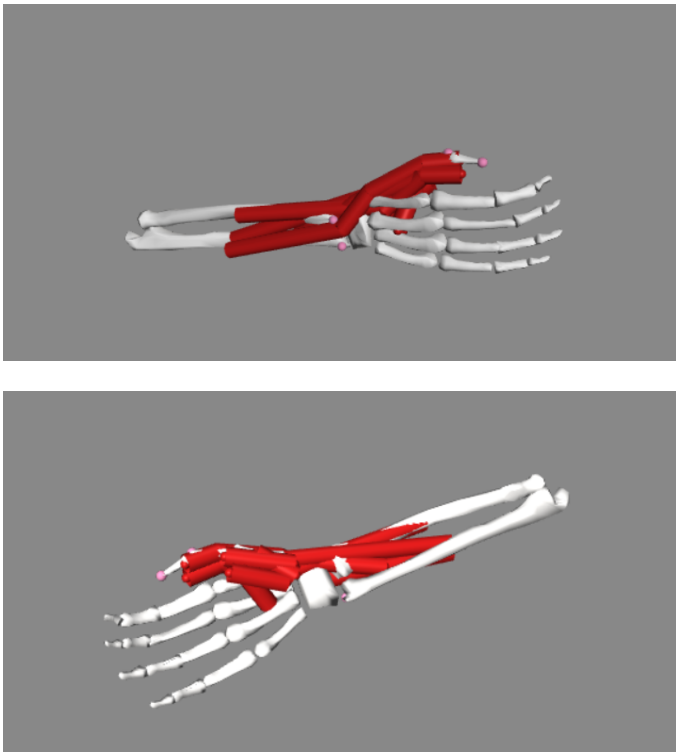

Fig. 4: The minimal Delft Hand and Wrist model in OpenSim. The model contains bony structures, muscles (indicated by the thick red lines) and the markerset (indicated by the small pink spheres). It should be noted that the carpal bones are combined to form one large bony structure. The top figure shows the dorsal side of the model. The bottom figure shows the palmar side of the model.

Wrist motion is limited to 20 degrees in all directions, i.e., flexion, extension, abduction and adduction, because the participants do not perform any wrist motion during the experiments. Finally, the Extensor Pollicis Longus (EPL) muscle in the original model has biomechanical properties that prevents the static optimization to find a feasible solution. Changing the tendon slack length of the EPL muscle solves this problem, because changing the tendon slack length of a muscle shifts where the muscle operates on the force-length curve [24].

The EPL tendon slack length is changed from 21 mm to 90 mm, according to values reported in literature [25]. The static optimization now works for the minimal model after applying these modifications on the original model.

B. Adjusted model

The adjusted model is obtained by changing the tendon slack length, maximum isometric force, and optimal fiber length values of the original model to values reported in Gonzalez et al. (1997) [26] and Kerkhof et al. (2018) [27]. Table A2 in the Appendix shows the changes that are made. The purpose of the adjusted model is to evaluate the effect of changing these musculoskeletal parameter values on the estimated muscle force.

Data analysis

The data analysis is completed using the following software: DeepLabCut [28], Anipose [29], OpenSim 4.1 [6], [12], and MATLAB R2019b.

A. DeepLabCut

The DeepLabCut software is used to develop a trained model that can identify and label marker positions on the 2D video recordings. A training dataset is obtained by manually labeling 720 frames (12 motions, six cameras per motion, 10 frames for each camera). Six marker points are labeled for each frame; thumb tip (TIP), first interphalangeal joint (IP1), first metacarpophalangeal joint (MCP1), first carpometacarpal joint (CMC1), radial styloid (RS), and the ground electrode representing the sixth marker, ulnar styloid (US). The marker points can be identified in the video recordings because they are marked on the hand of the participant using a black pencil before the start of the first recording. Figure 3 shows a snapshot taken from an arbitrary selected video recording in which the marker points can be recognized. After labeling, the training dataset is used to train the network for 200.000 iterations. The test and train errors were respectively 1.7 and 3.5 pixels. Figure 5 shows the results retrieved through applying the trained model on a new set of video recordings. The trained model is then used to create 2D labeled marker positions for all motions of all participants. The results are combined with the raw video recordings to create labeled videos. All labeled videos are inspected to verify if the recorded motion was tracked correctly.

B. Anipose

The 2D marker positions obtained from DeepLabCut and the calibration results are converted to a single file containing 3D marker positions using triangulation in Anipose. It is preferred to include as many cameras as possible in the triangulation process to increase its accuracy. A camera is excluded from the dataset when a marker is incorrectly tracked for more than five sequential frames. The recording is determined erroneous when more than three cameras are excluded from the dataset. All excluded trials are displayed in Table A3 in the Appendix.

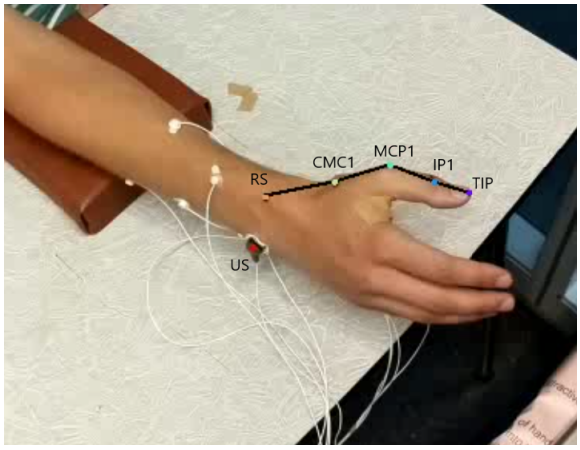

Fig. 5: The trained model is able to identify and label the marker positions on a new set of video recordings. The markers are indicated by the small colored dots. The solid black line is an imaginary skeleton for visual purposes only.

Configuration parameters for the triangulation in Anipose are a combination of default values and values retrieved from Van den Bogaart et al. (2021) [30], see Table A4 in the Appendix. The 3D position data resulting from the triangulation process is stored in a `.csv` file. This file is converted to a `.trc` storage file using MATLAB.

C. OpenSim

The OpenSim framework is used for the inverse dynamic analysis, i.e., the transformation from position data (the `.trc` file from MATLAB) to muscle forces estimated through static optimization. First, the model is scaled to match the kinematic data with the marker data using the OpenSim Scale tool. A static pose is created by taking the average of the marker positions in the first 0.1 seconds of the measurement data, when the hand is in the instructed neutral position. Marker pairs are created to define the bones between the markers, forming a 3D skeleton. Scale factors are computed by the Scale tool through measurement-based scaling using the marker pairs. For the inverse dynamics, the coordinates are filtered using a low-pass filter with a cut-off frequency of 5 Hz to remove high frequency noise [31].

The Static Optimization tool in OpenSim uses the minimum sum of the squared muscle activations as the cost function. The static optimization has the filtered results of the inverse kinematics as input. The output of the static optimization is a file containing the estimated muscle forces.

Thumb muscle moment arms computed in OpenSim are compared to simulated muscle moment arm values in Engelhardt et al. (2020) to find out if the moment arms in the Delft Hand and Wrist model correspond to moment arm values in a published hand model [32]. The hand model in Engelhardt et al. (2020) is created using the AnyBody Modelling System (AMS) platform.

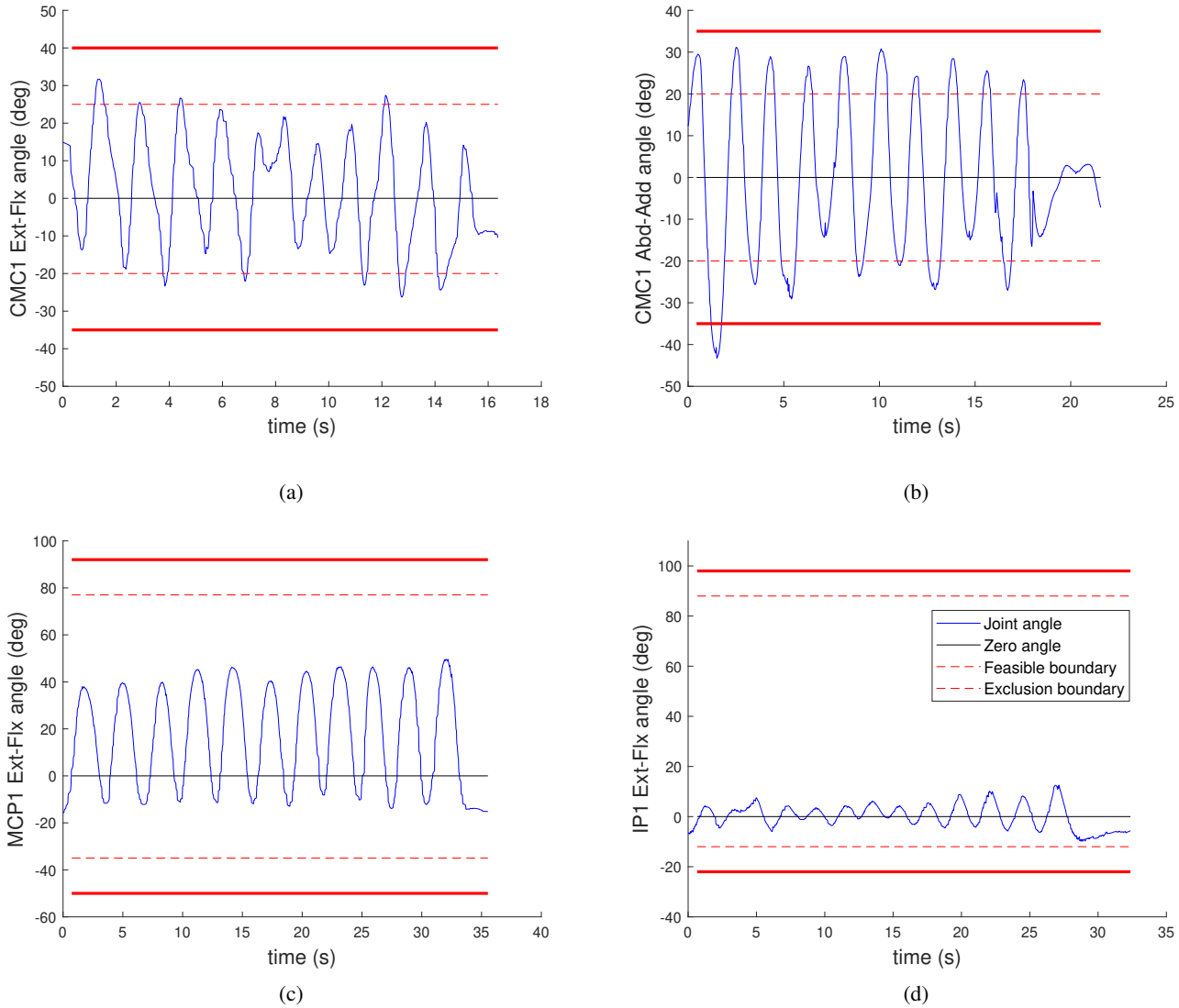

Fig. 6: Examples of joint angles and defined boundaries. The blue line indicates the joint angle, the dashed red lines indicate the boundary values reported in literature, the thick red lines indicate the exclusion boundaries and the thin black line indicates the transfer from abduction (negative) to adduction (positive) or from extension (negative) to flexion (positive). (a) CMC1 extension-flexion angle for Circle motion of participant 5. (b) CMC1 abduction-adduction angle for AA motion of participant 16. (c) MCP1 extension-flexion angle for OPP motion of participant 1. (d) IP1 extension-flexion angle for IP motion of participant 14.

D. MATLAB

Kinematic data

Joint angles resulting from the inverse kinematics are verified by checking if the values are within feasible range of motion bounds reported in literature. Trials are excluded if two or more joint angles showed results that fell 15 or more degrees outside of the defined feasible boundaries (see Table A3). Feasible boundary values are the following: CMC1 abduction-adduction [20:20 degrees] [33], CMC1 extension-flexion [20:25 degrees] [34], MCP1 extension-flexion [35:77 degrees] [35], and IP1 flexion-extension [12:88 degrees] [36]. Figure 6 shows joint angles for arbitrary selected participants and the defined boundaries.

The kinematic data is used to divide the signal into separate trials in a way that each trial contains a complete cycle of the motion of interest. Trials are defined by the most relevant joint angle for each motion; the IP1 angle is used for the IP motion, the MCP1 angle is used for the FE and the OPP motions, the CMC1 extension-flexion angle is used for the Circle motion, and the CMC1 abduction-adduction angle is used for the AA motion. Figure 7a shows the trial selection based on the CMC1 abduction-adduction angle of participant 16. The individual trials are plotted together in the same figure and trials that show visible outliers are removed. Trial 1 is excluded from the measurement, because the extension peak exceeds the defined exclusion boundary. Trial 10 is also excluded from the measurement, because there is no evident repetition of the

AA motion visibly present in this trial. Figure 7b shows the remaining trials for the AA motion of participant 16.

Muscle activity data

Individual muscle activity signals are extracted from the TMSi files and filtered using a fourth-order band-pass Butterworth filter (cut-off frequencies = 5 & 500 Hz) as recommended in literature [37], [38]. A linear envelope of each signal is created by rectifying using the absolute value of the filtered signal and applying a second-order low-pass Butterworth filter (cut-off frequency = 5 Hz) [38]. The MVC measurement is filtered using the same settings. The normalization of the signals is performed by dividing each sEMG signal by the maximum value found in the single MVC recording.

Validation

There are multiple methods to validate multibody musculoskeletal models [39]. The Delft Shoulder and Elbow Model was first validated by comparing the estimated muscle force-time curves to experimentally measured EMG signals, according to the method in van der Helm (1994) [40]. This method is a qualitative validation method, because the muscle force curves and EMG signals are compared and evaluated in terms of agreement to one another [41]. Quantitative validation expresses the correlation between two signals, so this type of validation uses numerical metrics. Quantitative validation in case of the Delft Shoulder and Elbow Model was performed using an instrumented shoulder endoprosthesis [42]. The endoprosthesis is able to measure the sum of frictional moments and contact forces in the glenohumoral joint, which was compared to the estimated forces in this joint by the model [43]. Unfortunately, no thumb muscle force data measured using an instrumented thumb endoprosthesis is currently available. Therefore, an other quantitative validation method is required. Żuk et al. (2018) state that sEMG can be used for the validation of estimated muscle forces with a so-called quantitative trend validation method [16]. The quantitative validation metrics in their study are based on the electromechanical delay offset and the Pearson correlation coefficient. The trend validation method by Żuk et al. (2018) is used in this work. The electromechanical delay is embedded in OpenSim through the activation time constant of 15 ms, which is within the reported range of 10-100 ms [7]. The Pearson correlation coefficients for the muscle activity and estimated muscle forces from the minimal model and the adjusted model are calculated and compared using MATLAB.

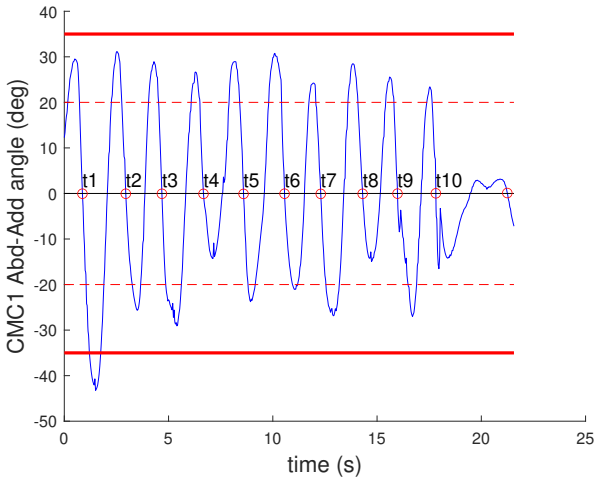

(a)

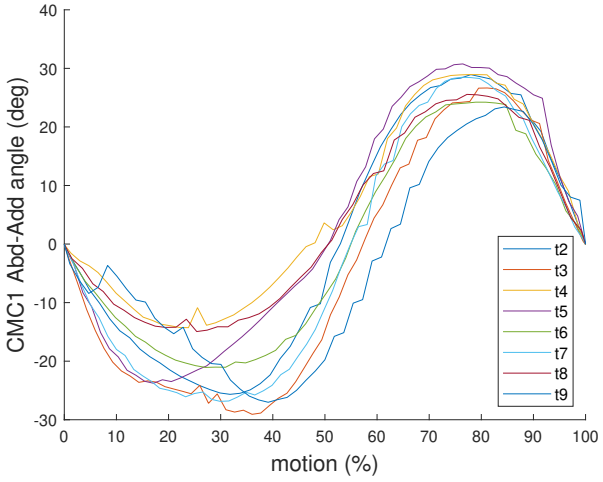

(b)

Fig. 7: (a) The locations of the cutting points based on the CMC1 abduction-adduction joint angle for the AA motion performed by participant 16. The red circles indicate the cutting point locations, the blue line indicates the joint angle, the dashed red lines indicate the boundary values reported in literature, the thick red lines indicate the exclusion boundaries and the thin black line indicates the transfer from abduction (negative) to adduction (positive). (b) The eight trials remaining after exclusion showing the CMC1 abduction-adduction angle for the AA motion of participant 16 versus % of the motion.

III. Results

Muscle moment arms

Muscle moment arms indicate the correctness of kinematics [32]. The muscle moment arms of the Delft Hand and Wrist model are computed by OpenSim based on the incorporated biomechanics. Figure 8 shows the calculated muscle moment arms of the EPB, EPL, FPB and FPL muscles in the adjusted model from maximal extension to maximal flexion around the CMC1 joint. The muscle moment arm values for the Delft Hand and Wrist model in Figure 8 do not show the clear distinction between thumb flexor and extensor muscles that is visible for the simulated muscle moment arm values from the AnyBody model [32]. Furthermore, the reported muscle moment arm value for the EPB muscle shows almost a constant value, while the muscle moment arm in the OpenSim model shows an increase for the EPB muscle. More muscle moment arm values of the Delft Hand and Wrist model compared to reported values from the AnyBody model are included in the Appendix (Figures A1 to A3).

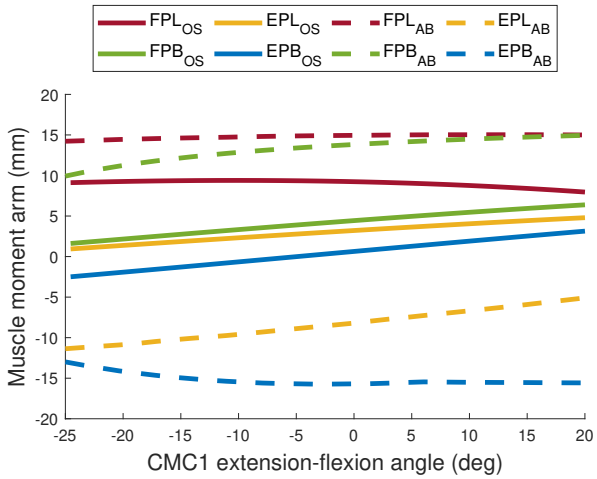

Fig. 8: Muscle moment arms of the FPL, FPB, EPL and EPB muscles from maximal extension to maximal flexion around the CMC1 joint for the adjusted model are represented by solid lines (OS = OpenSim model). Dashed lines represent the simulated results by Engelhardt et al. (2020) [32] (AB = AnyBody model).

Muscle activity

Figure 9 shows an example of the filtered muscle activity signals of the eight thumb muscles normalized to the maximal values found in the MVC measurement. The 10 repetitions are distinguished by counting the peaks in the figure. The individual trials of the sEMG signals obtained through separation based on joint angle are included in Figure A4 in the Appendix. Figure 10 shows the calculated mean and standard deviation of the sEMG trials for each thumb muscle.

Muscle forces

The muscle forces are normalized by dividing the estimated muscle forces by the maximum isometric force values displayed in Table A2 in the Appendix. Figure 11 shows the resulting normalized muscle force estimations for the AA motion of participant 16 for the adjusted model. The individual trials of the muscle force estimations obtained through separation based on joint angle are included in Figure A5 in the Appendix. Figure 12 shows the calculated mean and standard deviation of the estimated muscle force trials for each thumb muscle in the adjusted model.

Validation

Table I shows the mean and standard deviation taken from the Pearson correlation coefficient values for the eight thumb muscles per participant that performed the AA motion successfully. The majority of the mean correlation coefficient values for the adjusted model are higher than the mean correlation coefficient values for the minimal model. Still, there is no significant difference. The scale of the Pearson correlation coefficient is defined as follows: $0<r\leq0.19$ = very low correlation, $0.2\leq r\leq0.39$ = low correlation, $0.4\leq r\leq0.59$ = moderate correlation, $0.6\leq r\leq0.79$ = high correlation, and $0.8\leq r\leq1.0$ = very high correlation [44]. This means that three out of the 22 measurements of the AA motion could be classified as 'moderate correlation' and 19 measurements are classified as either 'low correlation' or 'very low correlation'.

IV. Discussion

In this work a quantitative validation of the thumb muscles in the Delft Hand and Wrist model in OpenSim is performed. Even though the estimated muscle forces of both the minimal and the adjusted model showed very low to moderate correlation to measured muscle activity data, this work offers potential for future studies on the Delft Hand and Wrist model by providing suggestions and reference data.

Muscle activity

Overall, the measured sEMG signals show a clear repetitive pattern in which the 10 trials are distinguished. The muscle activity in the first half of the AA motion (thumb abduction) in Figure 10 shows a peak in the thumb muscles responsible for thumb abduction (APB and APL muscles). The muscle responsible for thumb adduction (ADD muscle) shows a peak during the second half of the motion (thumb adduction). This means that the measured muscle activity corresponds to the activity that is expected when performing the instructed motion. Therefore, the data shows that the muscle activity was measured correctly.

Estimated muscle forces

At least the static optimization returned estimations of muscle forces for both the minimal and the adjusted model, where it was unable to find a feasible solution for the original model. However, the estimated muscle forces show less consistent peaks in Figure 11 in contrast to the clear peaks of the measured muscle activity for the same motion performed by the same participant. This means that the Static Optimization tool in OpenSim is inconsistent in allocating the force to the thumb muscles, because the kinematics are consistent.

A critical comment that should be made with regards to the Static Optimization tool in OpenSim is about the objective function that is used. For the objective function the minimization of the squared sum of muscle activations was used. This type of cost function is classified as a 'fatigue'-like cost function, because muscle fatigue is related to the percentage of active muscle fibers [45]. Fatigue-like cost functions minimize muscle fatigue as much as possible and are less associated with muscle volume [46], i.e., smaller muscles that can generate relatively more force are in favor of being selected for muscle force generation.

In Figure 11 the APL muscle produces relatively more muscle force when compared to the other muscles in this figure. The explanation for this is that the APL muscle has an advantageous combination of tendon slack length, optimal muscle fiber length and maximum isometric force parameter values with respect to the other thumb muscles, see Table A2. The APL muscle in the adjusted model can produce the

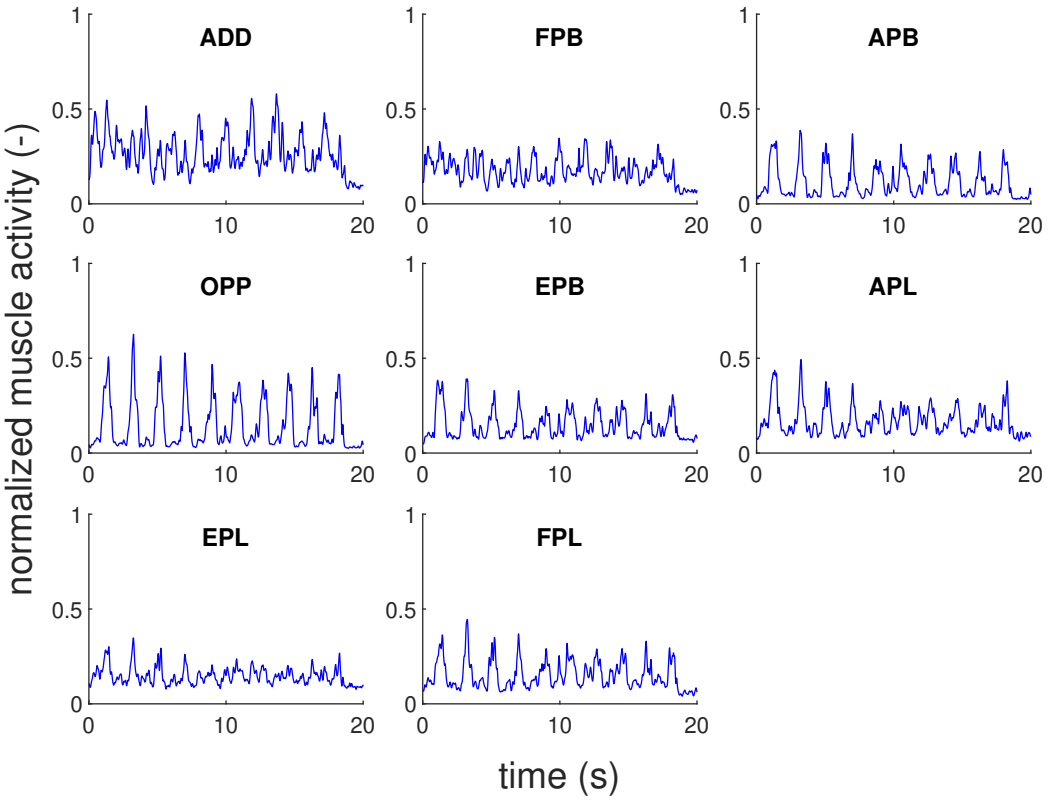

Fig. 9: EMG signals for the thumb muscles normalized to their MVC value for the AA motion performed by participant 16.

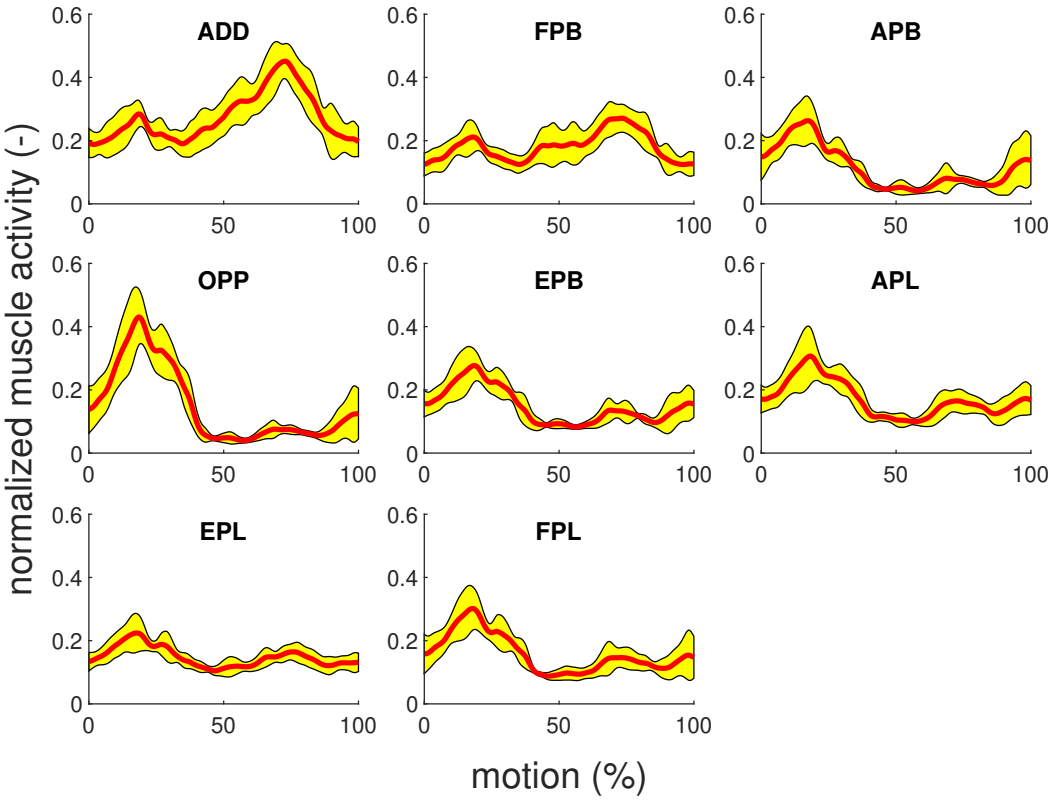

Fig. 10: Mean (thick red line) and standard deviation (yellow area) of the EMG trials for the thumb muscles for the AA motion performed by participant 16.

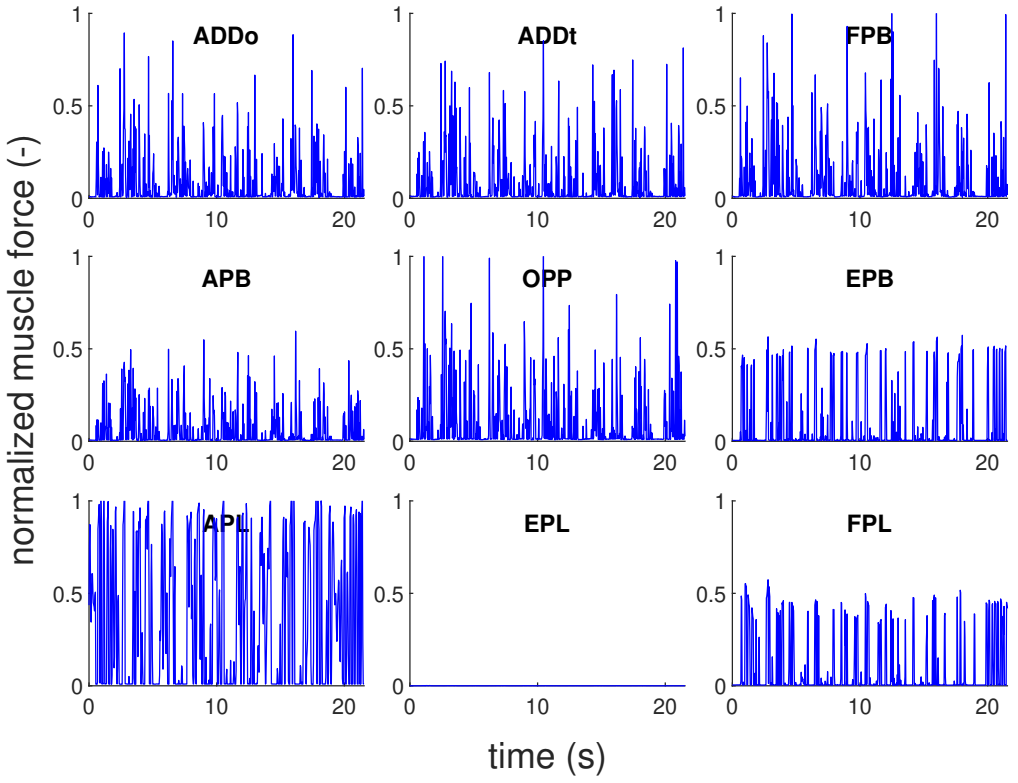

Fig. 11: Normalized muscle force estimations for the thumb muscles in the adjusted model for the AA motion performed by participant 16.

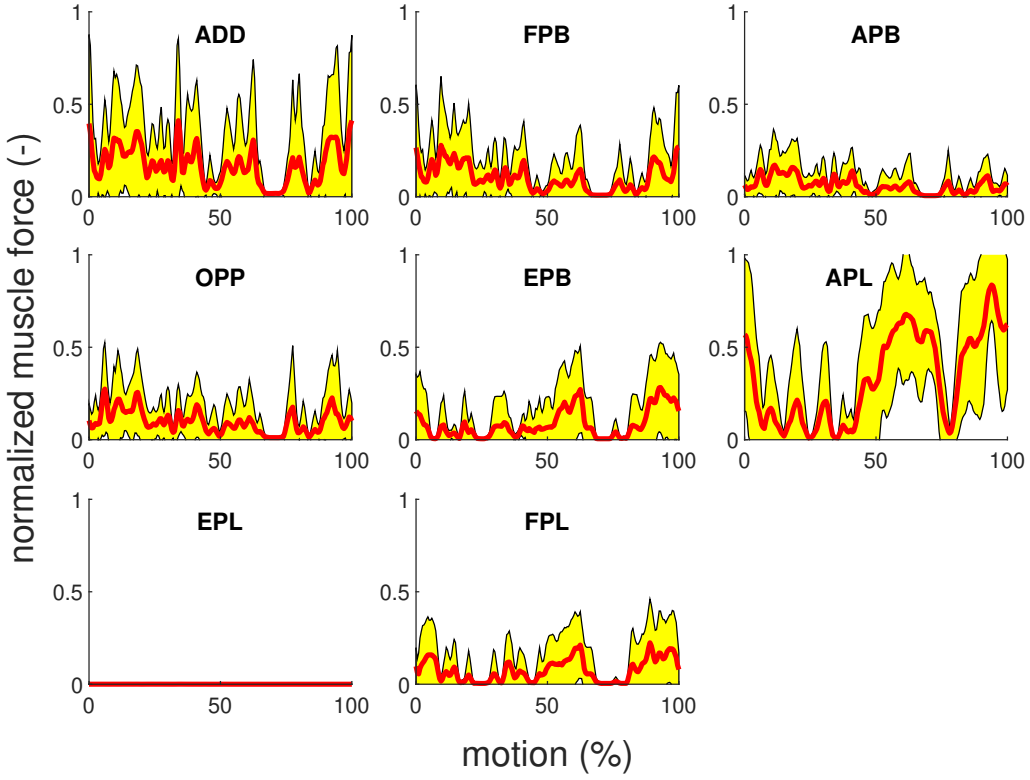

Fig. 12: Mean (thick red line) and standard deviation (yellow area) of the estimated muscle force trials for the thumb muscles for the AA motion performed by participant 16.

TABLE I: Mean Pearson correlation coefficient values (r) ± standard deviation for the AA motion.

Participant number	Minimal model ($\mu\pm$sd)	Adjusted model ($\mu\pm$sd)
1	0.28±0.18	0.13±0.09
4	0.22±0.16	0.43±0.14
5	0.20±0.15	0.29±0.15
6	0.23±0.24	0.29±0.21
7	0.19±0.14	0.19±0.10
8	0.26±0.16	0.24±0.19
10	0.26±0.11	0.17±0.18
13	0.14±0.13	0.21±0.09
15	0.25±0.11	0.30±0.26
16	0.42±0.22	0.45±0.16
18	0.38±0.15	0.25±0.22
Mean±sd	**0.26±0.16**	**0.27±0.16**

The first column contains the participant numbers of the participants that are included in the AA motion data analysis. The second column contains the mean Pearson correlation coefficient that expresses the correlation between the measured muscle activity and the estimated muscle forces of the minimal model. The third column shows the mean Pearson correlation coefficient that expresses the correlation between the measured muscle activity and the estimated muscle forces of the adjusted model.

same amount of force as the EPB and EPL muscle combined; 58 N versus 14 N and 44 N respectively. In addition, the APL optimal fiber length is only 5.8 mm. Therefore, it is assumed that the static optimization allocates muscle force to the APL muscle that should be allocated to the EPL muscle, hence the EPL muscle is granted no force in all the simulations.

Many more objective functions exist and no consensus is reached which objective function yield the most valid results [8]. Future research could study different objective functions in the static optimization using this model. Especially an energy-based cost function could provide promising results, because an energy-based cost function produced more realistic muscle activation predictions compared to a cost function based on the minimization of muscle forces [47].

Altogether, this work provides a basis for inverse dynamic muscle force estimation for the Delft Hand and Wrist model in OpenSim.

Muscle moment arms

Muscle moment arms influence the force distribution during static optimization [48]. The muscle moment arms in the Delft Hand and Wrist model do not show a clear difference between the flexor and extensor muscle moment arms when compared to simulated results using the AnyBody model (see Figure 8). Moreover, the muscle moment arm of the EPL muscle in the Delft Hand and Wrist model has a positive value from maximal extension to maximal flexion around the CMC1 joint in Figure 8. This means the EPL muscle in the Delft Hand and Wrist model is unable to perform extension around the CMC1 joint, which explains the absence of EPL muscle force in the estimations shown in Figure 11.

It is important that the muscle moment arms match reference values, which means there should be a more clear distinction between the thumb flexor and extensor muscle moment arms for the current Delft Hand and Wrist model and a negative value for the muscle moment arm of the EPL muscle. Adding wrapping surfaces or via points (points along the muscle path) to the model can alter muscle paths and hereby aid to match the muscle moment arm values of the model to the values reported in literature [5].

It is suggested to compare the muscle moment arms of the musculoskeletal model to reference values reported in literature prior to performing experiments. This suggestion is based on the fact that the muscle moment arms provide an indication for the correctness of the kinematics and play an important role during static optimization.

Validation

The estimated muscle forces by the model are compared to simultaneously measured muscle activity data in order to validate whether the model accurately represents reality. Validation was based on the AA motion in this work because 11 measurements were included for this motion, which was the most available data compared to other motions (see Table A3). For the AA motion the estimated muscle forces for both the minimal and the adjusted model shows very low to moderate correlation to the measured muscle activity data. This means the estimated muscle forces are not likely to be realistic estimations. The main explanation for this is that muscle force is granted to the wrong muscles during the static optimization in OpenSim. This can be overcome by (1) changing the objective function that is minimized in the static optimization, (2) altering the muscle moment arms to match muscle moment arms reported in literature or (3) by tuning the optimal fiber length, maximum isometric force and tendon slack length parameter values of the thumb muscles. The goal of the third option is to create a more advantageous position towards generation of muscle force for the thumb muscles that produce currently not enough force or no force at all. It is expected that the quantitative trend validation method used in this work results in higher correlation coefficient values if a better muscle force allocation is performed during static optimization.

In the paper by Melzner et al. (2022) the researchers used Cohen's kappa as a metric to describe the time difference of on- and offset points between measured and estimated muscle activity [49]. No arguments are made regarding the timing of muscle on- and off-set in this work, because the averaged muscle force estimations in Figure 12 do not show clear on- and offset points for the thumb muscles. Cohen's kappa is an interesting validation metric for when the thumb muscles show

clear on- and offset points after static optimization in future work.

This research pioneers the validation of the thumb muscles in the Delft Hand and Wrist model by setting a benchmark for future research. The current correlation coefficients show there is much to be gained and future studies should aim to improve the correlation between experimental muscle activity data and estimated muscle forces in the Delft Hand and Wrist model.

Kinematics

This work uses 3D kinematics as a result of markerless motion capture integrated with DeepLabCut and Anipose as the input for an inverse dynamics simulation. Table A3 shows that 33 out of 44 measurements that were imported from Anipose to OpenSim resulted in feasible kinematics because the data falls within the defined joint angle boundaries. This means that overall the kinematics are captured well, especially considering that the model does not include any constraints on the joint angles apart from the wrist motion. It is expected that even more measurements will become available once the dataset is increased by improving the trained model in DeepLabCut, i.e., decrease the difference between the test and train error when evaluating the trained model. All in all the ML-MoCap approach combined with the DeepLabCut and Anipose machine learning toolboxes presented in this work offers an alternative to conventional motion capture methods such as Kinect and Vicon Motion Capture [50].

Assumptions

Firstly, modeling assumptions were made in OpenSim. It is assumed that the selected muscles during the reduction of the original model are able to describe thumb motion accurately. This assumption is based on the origin and insertion of the selected muscles with regards to their function, see Table A1.

Another assumption is that the participants kept a constant velocity when performing the specific thumb motions. This assumption is important because of the signal cutting process. The individual trials are distinguished in a way that an entire revolution of the back and forth motion is described in percentage from 0% to 100%. This means that the velocity has to be constant for each trial in order to allow for comparison between each other and between trials of other participants. Using a rhythmic device, such as a metronome, in order to ensure constant velocity during the experiment would be a suggestion for future research. The joint angle curves in Figure 7b were used to verify if the participants were able to keep a constant velocity during the experiments. This visualization method offers a good alternative when a rhythmic device is unavailable.

Measuring muscle activity of the muscles in the hand or forearm is challenging, because the hand muscles are small and packed close together. The latter means that the micro-electrodes were located near each other, which leads to EMG signal contamination, otherwise referred to as crosstalk [51]. Other difficulties include the palpation of muscles located deeper within the palm of the hand and the fact that two out of the 18 participants experienced sweaty hands. This resulted in the micro-electrodes located on the intrinsic thumb muscle bellies not sticking to the palms of the participant, so they were put back into the correct position using elastic tape. It is assumed that the slight dangling of the wires of the eight micro-electrodes during the thumb motion does not produce noticeable additional noise. The dangling of the wires was reduced by taping the wires together in two groups of four.

Limitations

The main limitation of this work is the small sample size due to the amount of data that was excluded (see Appendix A3). Suggestions are provided on how to exclude less data. First, the cameras need a clear view of the segment that is being recorded in order for the DeepLabCut software to be able to track the motion. This means that irrelevant body parts should be kept off screen completely and that the motion of interest is performed in the direction that the cameras can see clearly. One recurring problem in the data analysis was that the DeepLabCut software tracked the wrong finger when marker points of the thumb moved out of sight of the cameras. The Anipose software could not recognise the incorrect marker tracking if it continued for multiple frames, which meant the data had to be excluded in that scenario. 10 trials per thumb motion seems enough repetitions. However, the trials were all within the same measurement. This means that all trials were eliminated if the measurement was excluded. Therefore, it is suggested to make multiple measurements of the same motion while each measurement contains multiple trials. It is assumed that a total of 18 participants is sufficient to provide enough results, based on equivalent studies [23], [49]. It should be mentioned that the dataset used in this study can be increased, i.e., data that is excluded in Table A3 can be saved. This applies to data that was excluded because of the DeepLabCut/Anipose marker misplacement, which can be fixed by manually labeling the videos or by improving the training model. It is decided to exclude the data in this work due to time restrictions, but future work could increase the dataset to have more data available for quantitative validation using sEMG.

Further limitations were mainly identified during the data analysis. For instead, the mass used in the Scale tool in OpenSim was 0.35384 kg by default. This number is low, especially since literature estimates the mean total hand plus forearm mass to be 1.55 kg [52]. An estimate of the total hand plus forearm mass for each participant could be computed based on percentage of total body mass [53], but no body mass data was measured for the participants in this experiment. However, it is assumed that the hand plus forearm mass difference between the Delft Hand and Wrist model and values reported in literature has a negligible effect on the results of the experiments in this work due to the fact that the experiments focused only on the thumb, which has a small contribution to the total hand plus forearm mass.

A different limitation arose from the fact that no markers were placed on the proximal ends of the ulna and radius. The lengths of the ulna and radius bones could not be scaled in

the Scale tool of OpenSim because of the absence of these markers, which could have affected the origin locations of the extrinsic thumb muscles. The insertions of the extrinsic thumb muscles are not affected by the scaling of the ulna and radius bones.

In the paper by Mirakhorlo et al. (2018) the authors discuss that the simplification of the wrist kinematics by combining the carpal bones to one single bony structure is a limitation of the model [11]. This simplification can influence the prediction of muscle moment arms around the wrist.

The model is not optimal yet. Nevertheless, the findings in this work are useful for the optimization of the current model and a promising approach for muscle force estimation and quantitative validation of the Delft Hand and Wrist model in OpenSim is presented.

Future work

A different approach to estimate the muscle forces is through the forward-dynamics time-dependent dynamic optimization to estimate muscle forces [18]. The inverse dynamics approach was used because of the additional computation time accompanied with the dynamic optimization approach. However, differences in estimated muscle forces of the upper extremity were found between the two approaches [54].

The Computed Muscle Control (CMC) approach is an alternative forward dynamics approach that tracks the experimental motion and computes the corresponding muscle excitations, while keeping the computational cost low [14]. The muscle forces can be predicted using the calculated muscle excitations as an input for a forward dynamic simulation. The CMC approach has an advantage over the dynamical optimization approach because it requires a single integration of the state equations, while the dynamic optimization approach requires thousands [55]. Future work should estimate the muscle forces using the CMC tool in OpenSim to find out if this results in different muscle force estimations compared to the results retrieved through static optimization.

To conclude, future work should aim to make the estimated thumb muscle forces more realistic by altering muscle moment arms, selecting a different objective function for the static optimization and/or tuning the optimal muscle fiber length, maximum isometric force and tendon slack length parameter values. This work provides recommendations regarding thumb muscle force estimation using inverse dynamic static optimization for future studies on the Delft Hand and Wrist model.

V. Conclusion

The current work presents a quantitative trend validation of the thumb muscles in a musculoskeletal hand model through comparing estimated muscle forces resulting from markerless motion capture to measured muscle activity data.

The quantitative trend validation based on the Pearson correlation coefficient was performed on the thumb muscles in the Delft Hand and Wrist model, because this model lacked a validation for the thumb muscles. The achieved correlation between the estimated muscle forces and experimentally measured muscle activity data for both the minimal model and the adjusted model was very low to moderate, meaning that the estimated muscle forces are unrealistic. Nevertheless, a basis is created for the validation of the thumb muscles in the Delft Hand and Wrist model.

The correlation coefficient values for the adjusted model were slightly higher, but not significant. Therefore, the model is insensitive to changing the maximum isometric force, tendon slack length and optimal muscle fiber length values to values reported in literature.

The ultimate goal is to make the Delft Hand and Wrist model more representative of reality and to make the model available online for answering upcoming research questions. The next step towards achieving this goal is to alter the thumb muscle moment arms to accomplish a better match with thumb muscle moment arm values reported in literature. Then the dataset of this study should be extended by fixing previously excluded data through manually labeling the recordings. The muscle forces are estimated again and quantitative validation is performed using the experimental muscle activity data from this experiment. The minimal model is expanded by including the removed muscles from the original Delft Hand and Wrist model if the estimated muscle forces show a high correlation to the measured muscle activity data. This work offers a basis for future muscle force estimation using the Delft Hand and Wrist model, as well as an extensive dataset that can be used for simulations and validation.

Acknowledgments

The author would like to thank his supervisor Winfred Mugge and daily supervisor Jinne Geelen for their motivation and unconditional support. The author also wants to acknowledge Judith Cueto Fernández, Mojtaba Mirakhorlo, Frans Van der Helm and Ajay Seth for their time and initial guidance on how to use the model. Finally the author would like to thank the students of the NMC Lab for their valuable input during the meetings every other week.

References

[1] J. Maw, K. Y. Wong, and P. Gillespie, "Hand anatomy," *British Journal of Hospital Medicine*, vol. 77, no. 3, pp. C34–C40, 2016.

[2] F. Chen Chen, S. Appendino, A. Battezzato, A. Favetto, M. Mousavi, and F. Pescarmona, "Constraint study for a hand exoskeleton: human hand kinematics and dynamics," *Journal of Robotics*, vol. 2013, 2013.

[3] N. Sun, G. Li, and L. Cheng, "Design and validation of a self-aligning index finger exoskeleton for post-stroke rehabilitation," *IEEE Transactions on Neural Systems and Rehabilitation Engineering*, vol. 29, pp. 1513–1523, 2021.

[4] (2022) World health organization, *Stroke, Cerebrovascular accident*. Accessed: 25.01.2022. [Online]. Available: http://www.emro.who.int/health-topics/stroke-cerebrovascular-accident/index.html

[5] K. R. S. Holzbaur, W. M. Murray, and S. L. Delp, "A model of the upper extremity for simulating musculoskeletal surgery and analyzing neuromuscular control," *Annals of biomedical engineering*, vol. 33, no. 6, pp. 829–840, 2005.

[6] S. L. Delp, F. C. Anderson, A. S. Arnold, P. Loan, A. Habib, C. T. John, E. Guendelman, and D. G. Thelen, "Opensim: open-source software to create and analyze dynamic simulations of movement," *IEEE transactions on biomedical engineering*, vol. 54, no. 11, pp. 1940–1950, 2007.

[7] T. S. Buchanan, D. G. Lloyd, K. Manal, and T. F. Besier, "Neuromusculoskeletal modeling: estimation of muscle forces and joint moments and movements from measurements of neural command," *Journal of applied biomechanics*, vol. 20, no. 4, pp. 367–395, 2004.

[8] A. Erdemir, S. McLean, W. Herzog, and A. J. van den Bogert, "Model-based estimation of muscle forces exerted during movements," *Clinical biomechanics*, vol. 22, no. 2, pp. 131–154, 2007.

[9] R. Happee, "Inverse dynamic optimization including muscular dynamics, a new simulation method applied to goal directed movements," *Journal of biomechanics*, vol. 27, no. 7, pp. 953–960, 1994.

[10] D. Tsirakos, V. Baltzopoulos, and R. Bartlett, "Inverse optimization: functional and physiological considerations related to the force-sharing problem," *Critical Reviews™ in Biomedical Engineering*, vol. 25, no. 4-5, 1997.

[11] M. Mirakhorlo, N. Van Beek, M. Wesseling, H. Maas, H. E. J. Veeger, and I. Jonkers, "A musculoskeletal model of the hand and wrist: model definition and evaluation," *Computer methods in biomechanics and biomedical engineering*, vol. 21, no. 9, pp. 548–557, 2018.

[12] A. Seth, J. L. Hicks, T. K. Uchida, A. Habib, C. L. Dembia, J. J. Dunne, C. F. Ong, M. S. DeMers, A. Rajagopal, M. Millard, S. R. Hamner, E. M. Arnold, J. R. Yong, S. K. Lakshmikanth, M. A. Sherman, J. P. Ku, and S. L. Delp, "Opensim: Simulating musculoskeletal dynamics and neuromuscular control to study human and animal movement," *PLoS computational biology*, vol. 14, no. 7, p. e1006223, 2018.

[13] M. Mirakhorlo, J. M. A. Visser, B. A. A. X. Goislard de Monsabert, F. C. T. Van der Helm, H. Maas, and H. E. J. Veeger, "Anatomical parameters for musculoskeletal modeling of the hand and wrist," *International Biomechanics*, vol. 3, no. 1, pp. 40–49, 2016.

[14] D. G. Thelen, F. C. Anderson, and S. L. Delp, "Generating dynamic simulations of movement using computed muscle control," *Journal of biomechanics*, vol. 36, no. 3, pp. 321–328, 2003.

[15] E. T. Emerson, T. J. Krizek, and D. P. Greenwald, "Anatomy, physiology, and functional restoration of the thumb." *Annals of plastic surgery*, vol. 36, no. 2, pp. 180–191, 1996.

[16] M. Żuk, M. Syczewska, and C. Pezowicz, "Use of the surface electromyography for a quantitative trend validation of estimated muscle forces," *Biocybernetics and Biomedical Engineering*, vol. 38, no. 2, pp. 243–250, 2018.

[17] E. De Pieri, M. E. Lund, A. Gopalakrishnan, K. P. Rasmussen, D. E. Lunn, and S. J. Ferguson, "Refining muscle geometry and wrapping in the tlem 2 model for improved hip contact force prediction," *PloS one*, vol. 13, no. 9, p. e0204109, 2018.

[18] F. C. Anderson and M. G. Pandy, "Static and dynamic optimization solutions for gait are practically equivalent," *Journal of biomechanics*, vol. 34, no. 2, pp. 153–161, 2001.

[19] J. E. Geelen, M. P. Branco, N. F. Ramsey, F. C. T. van der Helm, W. Mugge, and A. C. Schouten, "Markerless motion capture: Ml-mocap, a low-cost modular multi-camera setup," in *2021 43rd Annual International Conference of the IEEE Engineering in Medicine & Biology Society (EMBC)*. IEEE, 2021, pp. 4859–4862.

[20] Seniam guidelines. Accessed: September 2021. [Online]. Available: ⟨http://www.seniam.org/⟩

[21] Vh dissector. Accessed: September 2021. [Online]. Available: ⟨http://www.vhdissector.com/⟩

[22] Anipose realease 0.8.1. Accessed: January 2022. [Online]. Available: ⟨https://anipose.readthedocs.io/_/downloads/en/latest/pdf/⟩

[23] P. Karashchuk, K. L. Rupp, E. S. Dickinson, S. Walling-Bell, E. Sanders, E. Azim, B. W. Brunton, and J. C. Tuthill, "Anipose: a toolkit for robust markerless 3d pose estimation," *Cell reports*, vol. 36, no. 13, p. 109730, 2021.

[24] J. L. Hicks, T. K. Uchida, A. Seth, A. Rajagopal, and S. L. Delp, "Is my model good enough? best practices for verification and validation of musculoskeletal models and simulations of movement," *Journal of biomechanical engineering*, vol. 137, no. 2, 2015.

[25] I. A. Khan and M. Varacallo, "Anatomy, shoulder and upper limb, hand extensor pollicis longus muscle," *StatPearls [Internet]*, 2021.

[26] R. V. Gonzalez, T. S. Buchanan, and S. L. Delp, "How muscle architecture and moment arms affect wrist flexion-extension moments," *Journal of biomechanics*, vol. 30, no. 7, pp. 705–712, 1997.

[27] F. D. Kerkhof, T. Van Leeuwen, and E. E. Vereecke, "The digital human forearm and hand," *Journal of anatomy*, vol. 233, no. 5, pp. 557–566, 2018.

[28] T. Nath, A. Mathis, A. C. Chen, A. Patel, M. Bethge, and M. W. Mathis, "Using deeplabcut for 3d markerless pose estimation across species and behaviors," *Nature protocols*, vol. 14, no. 7, pp. 2152–2176, 2019.

[29] A. Mathis, P. Mamidanna, K. M. Cury, T. Abe, V. N. Murthy, M. W. Mathis, and M. Bethge, "Deeplabcut: markerless pose estimation of user-defined body parts with deep learning," *Nature neuroscience*, vol. 21, no. 9, pp. 1281–1289, 2018.

[30] M. van den Bogaart, S. M. Bruijn, J. Spildooren, J. H. van Dieën, and P. Meyns, "Effects of age and surface instability on the control of the center of mass," *bioRxiv*, 2021.

[31] S. Schreven, P. J. Beek, and J. B. J. Smeets, "Optimising filtering parameters for a 3d motion analysis system," *Journal of Electromyography and Kinesiology*, vol. 25, no. 5, pp. 808–814, 2015.

[32] L. Engelhardt, M. Melzner, L. Havelkova, P. Fiala, P. Christen, S. Dendorfer, and U. Simon, "A new musculoskeletal anybody™ detailed hand model," *Computer methods in biomechanics and biomedical engineering*, pp. 1–11, 2020.

[33] T. D. Niehues and A. D. Deshpande, "Variable thumb moment arm modeling and thumb-tip force production of a human-like robotic hand," *Journal of biomechanical engineering*, vol. 139, no. 10, 2017.

[34] J. Z. Wu, K. An, R. G. Cutlip, M. E. Andrew, and R. G. Dong, "Modeling of the muscle/tendon excursions and moment arms in the thumb using the commercial software anybody," *Journal of biomechanics*, vol. 42, no. 3, pp. 383–388, 2009.

[35] R. Yoshida, H. O. House, R. M. Patterson, M. A. Shah, and S. F. Viegas, "Motion and morphology of the thumb metacarpophalangeal joint," *The Journal of hand surgery*, vol. 28, no. 5, pp. 753–757, 2003.

[36] M. J. Barakat, J. Field, and J. Taylor, "The range of movement of the thumb," *Hand*, vol. 8, no. 2, pp. 179–182, 2013.

[37] C. J. De Luca, L. D. Gilmore, M. Kuznetsov, and S. H. Roy, "Filtering the surface emg signal: Movement artifact and baseline noise contamination," *Journal of biomechanics*, vol. 43, no. 8, pp. 1573–1579, 2010.

[38] W. Rose, "Electromyogram analysis," *Online course material. University of Delaware. Retrieved January 2022*, vol. 5, p. 2016, 2011.

[39] M. E. Lund, M. de Zee, M. S. Andersen, and J. Rasmussen, "On validation of multibody musculoskeletal models," *Proceedings of the Institution of Mechanical Engineers, Part H: Journal of Engineering in Medicine*, vol. 226, no. 2, pp. 82–94, 2012.

[40] F. C. T. Van der Helm, "A finite element musculoskeletal model of the shoulder mechanism," *Journal of biomechanics*, vol. 27, no. 5, pp. 551–569, 1994.

[41] V. T. Inman, H. J. Ralston, J. B. d. C. M. Saunders, M. B. B. Feinstein, and E. W. Wright Jr., "Relation of human electromyogram to muscular tension," *Electroencephalography and clinical neurophysiology*, vol. 4, no. 2, pp. 187–194, 1952.

[42] A. A. Nikooyan, H. E. J. Veeger, P. Westerhoff, F. Graichen, G. Bergmann, and F. C. T. Van der Helm, "Validation of the delft shoulder and elbow model using in-vivo glenohumeral joint contact forces," *Journal of biomechanics*, vol. 43, no. 15, pp. 3007–3014, 2010.

[43] P. Westerhoff, F. Graichen, A. Bender, A. Rohlmann, and G. Bergmann, "An instrumented implant for in vivo measurement of contact forces and contact moments in the shoulder joint," *Medical Engineering & Physics*, vol. 31, no. 2, pp. 207–213, 2009.

[44] M. Selvanathan, N. Jayabalan, G. K. Saini, M. Supramaniam, and N. Hussin, "Employee productivity in malaysian private higher educational institutions," *PalArch's Journal of Archaeology of Egypt/Egyptology*, vol. 17, no. 3, pp. 66–79, 2020.

[45] M. Ackermann and A. J. Van den Bogert, "Optimality principles for model-based prediction of human gait," *Journal of biomechanics*, vol. 43, no. 6, pp. 1055–1060, 2010.

[46] L. J. Holmberg and A. Klarbring, "Muscle decomposition and recruitment criteria influence muscle force estimates," *Multibody system dynamics*, vol. 28, no. 3, pp. 283–289, 2012.

[47] M. Praagman, "Muscle load sharing," Ph.D. dissertation, PhD thesis, VU Amsterdam, 2008.

[48] S. Heintz and E. M. Gutierrez-Farewik, "Static optimization of muscle forces during gait in comparison to emg-to-force processing approach," *Gait & posture*, vol. 26, no. 2, pp. 279–288, 2007.

[49] M. Melzner, L. Engelhardt, U. Simon, and S. Dendorfer, "Electromyography-based validation of a musculoskeletal hand model," *Journal of Biomechanical Engineering*, vol. 144, no. 2, 2022.

[50] F. Schlagenhauf, S. Sreeram, and W. Singhose, "Comparison of kinect and vicon motion capture of upper-body joint angle tracking," in *2018 IEEE 14th International Conference on Control and Automation (ICCA)*. IEEE, 2018, pp. 674–679.

[51] Y. Kong, M. S. Hallbeck, and M. Jung, "Crosstalk effect on surface electromyogram of the forearm flexors during a static grip task," *Journal of Electromyography and Kinesiology*, vol. 20, no. 6, pp. 1223–1229, 2010.

[52] V. Katch and E. Gold, "Normative data for body segment weights, volumes, and densities in cadaver and living subjects," *Research Quarterly. American Alliance for Health, Physical Education and Recreation*, vol. 47, no. 3, pp. 542–547, 1976.

[53] S. Plagenhoef, F. G. Evans, and T. Abdelnour, "Anatomical data for analyzing human motion," *Research quarterly for exercise and sport*, vol. 54, no. 2, pp. 169–178, 1983.
[54] M. M. Morrow, J. W. Rankin, R. R. Neptune, and K. R. Kaufman, "A comparison of static and dynamic optimization muscle force predictions during wheelchair propulsion," *Journal of biomechanics*, vol. 47, no. 14, pp. 3459–3465, 2014.
[55] D. G. Thelen and F. C. Anderson, "Using computed muscle control to generate forward dynamic simulations of human walking from experimental data," *Journal of biomechanics*, vol. 39, no. 6, pp. 1107–1115, 2006.
[56] F. Paulsen and J. Waschke, *Sobotta, Atlas van de menselijke anatomie Deel 1: Algemene anatomie en bewegingsapparaat*. Houten: Bohn Stafleu van Loghum, 2011.

APPENDIX
TABLES

TABLE A1: Thumb muscle characteristics.

Muscle	**Origin**	**Insertion**	**Function**
Flexor Pollicis Longus (FPL)	Halfway anterior surface radius and interosseous membrane	Base of distal phalanx 1	Flexion thumb
Flexor Pollicis Brevis (FPB)	Trapezium and flexor retinaculum	Proximal phalanx 1	Flexion thumb at MCP1 joint
Extensor Pollicis Longus (EPL)	Halway posterior surface ulna and interosseous membrane	Distal phalanx 1	Extension thumb
Extensor Pollicis Brevis (EPB)	Radius and interosseous membrane	Proximal phalanx thumb	Extension thumb at MCP1 joint
Abductor Pollicis Longus (APL)	Ulna, radius and interosseous membrane	Metacarpal 1	Abduction and extension thumb
Abductor Pollicis Brevis (APB)	Transverse carpal ligament, scaphoid and trapezium bones	Base of proximal phalanx 1	Abduction thumb at CMC1 and MCP1 joint
Adductor Pollicis (ADD)	Basis and anterior side metacarpal 3, basis of metacarpal 2 and trapezoid and capitate bones	Base of PP1 and ulnar sesamoid	Adduction thumb at CMC1 joint
Opponens Pollicis (OPP)	Trapezium and transverse carpal ligament	Radial side of metacarpal 1	Opposition thumb

Table containing the eight muscles responsible for thumb motion and their origin, insertion and function. The anatomical information was retrieved from: Sobotta deel 1 [56].

TABLE A2: Minimal and adjusted model parameter values.

	Opt. Fiber length (mm)		Max. Iso Force (N)		Tendon slack length (mm)	
Muscles	Minimal	Adjusted	Minimal	Adjusted	Minimal	Adjusted
APB	3	**5**	9.7	9.7	2.5	2.5
APL	5.1	**5.8**	16.65	**58**	106	106
ADDo	15	**30.7**	19.4	19.4	20	**24**
ADDt	20	**40.8**	8	8	25	**1**
EPB	50	**68**	13.5	**14**	110	110
EPL	44	**54**	159	**44**	90	90
FPB	20	**56**	5	5	20	**15**
FPL	55	55	56	**62**	140	140
OPP	20	**30**	7.65	7.65	9.9	**1**

Optimal fiber length, maximal isometric force and tendon slack length values for the minimal model and the adjusted model. Changes for the adjusted model relative to the minimal model are shown in bold.

TABLE A3: All measurement data.

Participant	FE	TIP FE	AA	OPP	Circle
1	X(A)	O	O	O	X(M)
2	X(A)	X(A)	X(A)	X(A)	X(B)
3	X(A)	O	X(A)	X(A)	X(A)
4	X(B)	X(A)	O	X(A)	X(A)
5	X(B)	O	O	O	O
6	X(B)	O	O	X(B)	O
7	X(A)	X(A)	O	X(A)	O
8	X(A)	X(B)	O	X(A)	X(B)
9	X(A)	X(B)	X(B)	X(A)	O
10	O	O	O	X(A)	O
11	X(A)	X(A)	X(A)	X(A)	O
12	O	X(M)	X(M)	O	O
13	X(B)	O	O	X(M)	X(M)
14	X(A)	O	X(A)	X(A)	O
15	X(A)	X(A)	O	X(A)	X(A)
16	X(A)	X(A)	O	X(A)	O
17	X(B)	X(A)	X(M)	X(A)	X(A)
18	X(A)	X(A)	O	X(A)	O
Total included	**2**	**7**	**11**	**3**	**10**

Included data marked with O, excluded data marked with X. Within brackets the reason for exclusion is indicated: (A) = Anipose placed markers on wrong location. (B) = Kinematic data is out of feasible bounds. (M) = Missing data.

TABLE A4: Configuration parameters for the triangulation in Anipose.

3D filter parameter	Value
score_threshold	0.8
reproj_error_threshold	2
scale_length	10
scale_length_weak	2
scale_smooth	25
n_deriv_smooth	2

Parameters were a combination of default values and values retrieved from Van den Bogaart et al. (2021) [30]. Reprojection error threshold has pixels as unit, the other parameters are dimensionless.

FIGURES

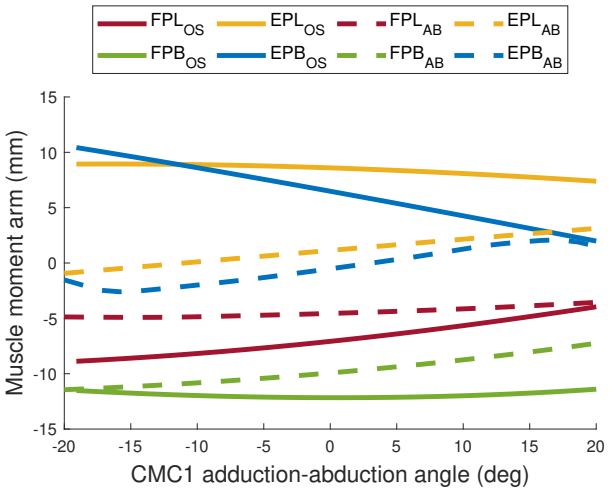

Fig. A1: Muscle moment arms of the FPL, FPB, EPL and EPB muscles from maximal adduction to maximal abduction around the CMC1 joint for the adjusted model are represented by solid lines (OS = OpenSim model). Dashed lines represent the simulated results by Engelhardt et al. (2020) [32] (AB = AnyBody model).

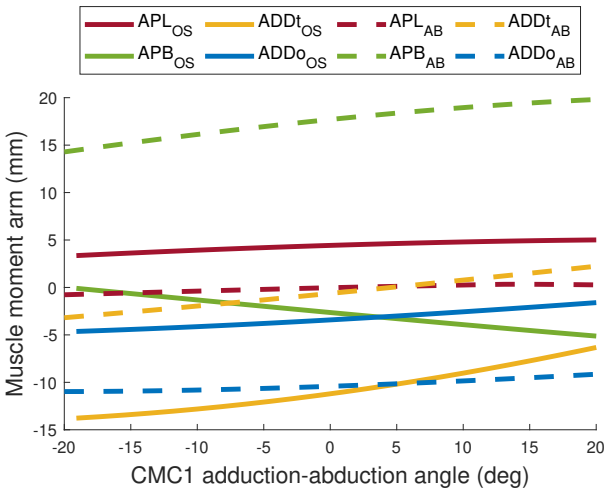

Fig. A2: Muscle moment arms of the APL, APB, ADDt and ADDo muscles from maximal adduction to maximal abduction around the CMC1 joint for the adjusted model are represented by solid lines (OS = OpenSim model). Dashed lines represent the simulated results by Engelhardt et al. (2020) [32] (AB = AnyBody model).

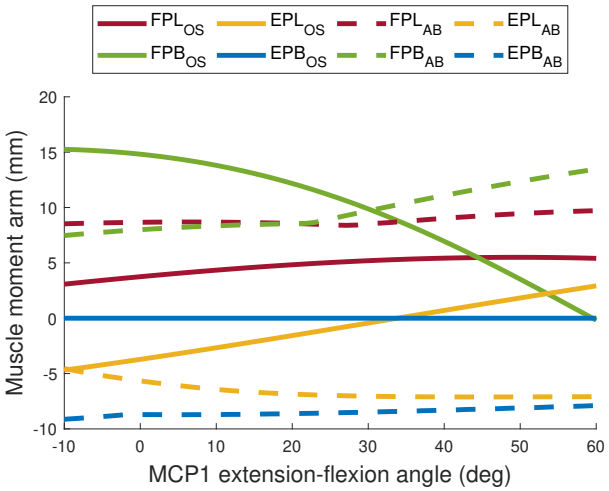

Fig. A3: Muscle moment arms of the FPL, FPB, EPL and EPB muscles from maximal extension to maximal flexion around the MCP1 joint for the adjusted model are represented by solid lines (OS = OpenSim model). Dashed lines represent the simulated results by Engelhardt et al. (2020) [32] (AB = AnyBody model).

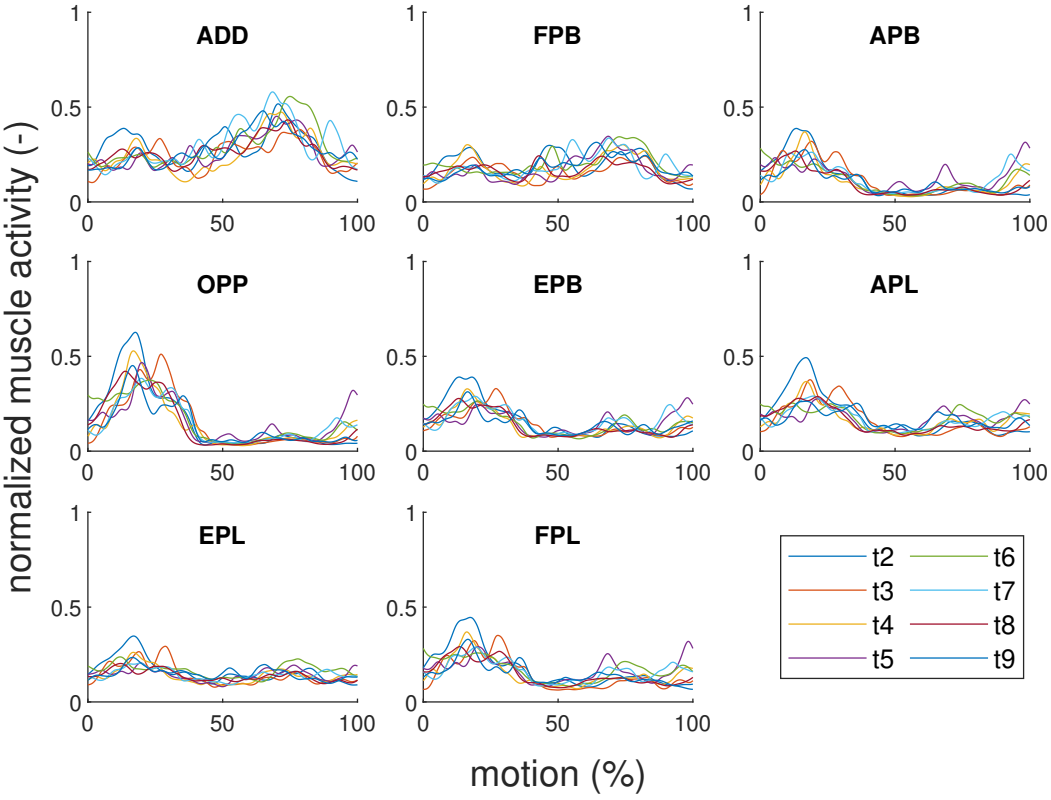

Fig. A4: Individual sEMG trials for the thumb muscles for the AA motion performed by participant 16. A total of two trials were removed because they did not provide a clear trajectory of the motion.

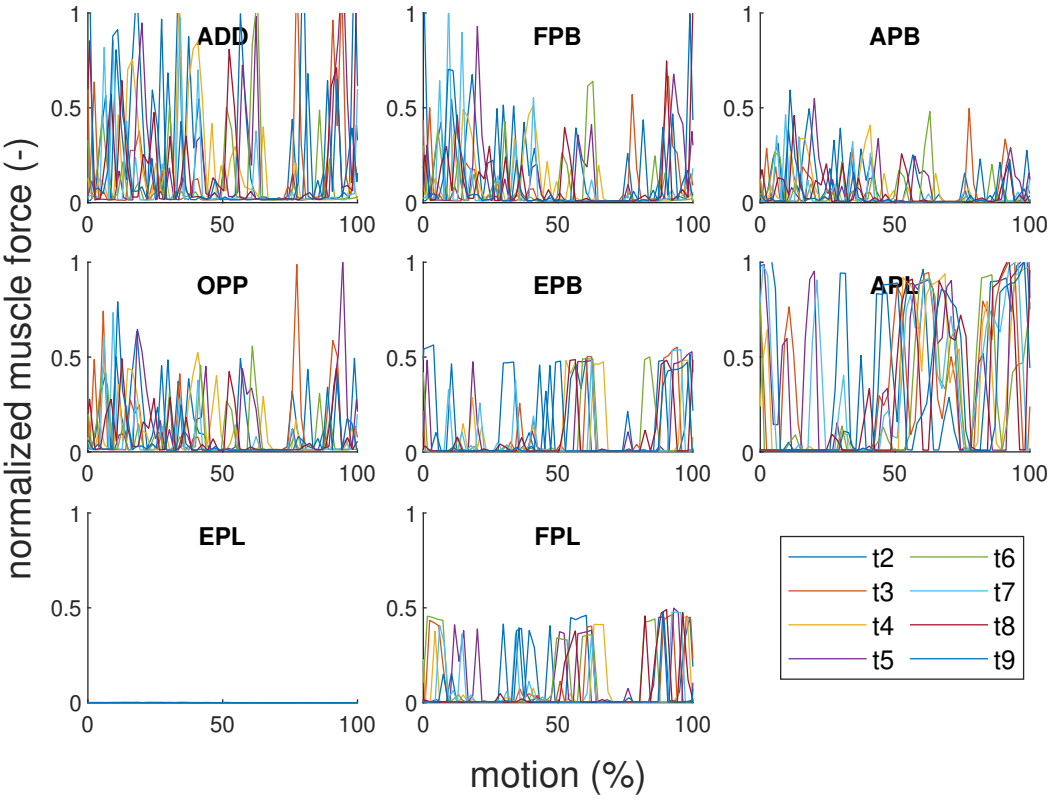

Fig. A5: Individual muscle force estimation trials for the thumb muscles in the adjusted model for the AA motion performed by participant 16. A total of two trials were removed because they did not provide a clear trajectory of the motion.